



Micro-scale twistable organic field effect transistors and complementary inverters fabricated by orthogonal photolithography on flexible polyimide substrate

Jingon Jang^a, Younggul Song^a, Daekyoung Yoo^a, Tae-Young Kim^a, Seok-Heon Jung^b,
Seunghun Hong^a, Jin-Kyun Lee^{b,*}, Takhee Lee^{a,*}

^a Department of Physics and Astronomy, and Institute of Applied Physics, Seoul National University, Seoul 151-747, South Korea

^b Department of Polymer Science and Engineering, Inha University, Incheon 402-751, South Korea

ARTICLE INFO

Article history:

Received 22 June 2014

Received in revised form 8 August 2014

Accepted 12 August 2014

Available online 26 August 2014

Keywords:

Organic field effect transistor

Flexible electronics

Twistable device

Complementary inverter

ABSTRACT

We fabricated micro-scale organic field effect transistors (OFETs) and complementary inverters on a twistable polyimide (PI) substrate by applying orthogonal photolithography. By applying a highly fluorinated photoresist and development solvent, it becomes possible to create organic electronic devices with a micro-scale channel length without damaging the underlying polymer films. The 3 μm-channel twistable pentacene OFET devices and complementary inverters created using p-type pentacene and n-type copper hexadecafluorophthalocyanine exhibited stable electrical characteristics from flat to twist configurations (angle of up to ~50°). The realization of twistable micro-scale OFETs and inverter devices on a PI substrate may enable the production of functioning organic devices in practical, flexible configurations.

© 2014 Elsevier B.V. All rights reserved.

1. Introduction

Recently, organic electronic devices, including organic field effect transistors (OFETs), non-volatile memories, light-emitting diodes, and solar cells, have received considerable attention based on their excellent advantages, such as a simple device structure, an easy and low-cost fabrication process, printability, flexibility, material variety, and a myriad of potential applications [1–9]. Because of the vast selection of organic materials for electronic devices, a variety of device fabrication processes have been demonstrated, including thermal evaporation, spin-coating, drop-casting, inkjet printing, and roll-to-roll printing [10–15]. However, in spite of these merits, for most organic electronic devices, it remains difficult to apply the conventional

photolithographic technology, which is widely used to create micro-scale high-density inorganic devices, because the existing organic solvents for photolithographic processing are not sufficiently selective to dissolve only the photoresist and not the organic layers [16,17]. To solve this problem, fluorinated solvents are good candidates for the photolithographic processing of organic electronic devices because highly fluorinated materials generally have orthogonal properties to those of most organic materials, regardless of their polarity. The orthogonality is required to protect the polymer films during the addition of lithographic chemicals [18]. Among the various fluorinated solvents that do not dissolve the organic materials, segregated hydrofluoroethers (HFEs) have attracted great attention because of their outstanding properties, such as their non-flammability, lack of ozone-depletion potential, low global warming potential, and low toxicity for humans. For this reason, the use of HFEs as photolithographic solvents has

* Corresponding authors. Tel.: +82 2 880 4269.

E-mail addresses: jk136@inha.ac.kr (J.-K. Lee), tleee@snu.ac.kr (T. Lee).

been studied extensively besides being used as eco-friendly refrigerants and cleaning solvents [18–22].

Because the technological progress of user-friendly devices will be a major focus in future electronics, the flexibility of organic materials and electronic devices has become more important for their application in foldable and wearable electronic devices. To ensure that flexible organic electronic devices are the core elements in future electronics, flexible devices should work stably not only in bending conditions but also in complex twist configurations that occur in practical use [23–25]. As an example, our group has recently reported twistable non-volatile organic resistive memory devices [26].

In this study, we fabricated micro-scale twistable OFET devices and complementary inverters consisting of pentacene and copper hexadecafluorophthalocyanine ($F_{16}CuPc$) on a flexible polyimide (PI) substrate. The micro-scale device fabrication of the OFETs was made possible by applying orthogonal photolithography using the HFE photolithographic solvents and a compatible highly fluorinated photoresist solution. The 3 μm -channel twistable OFET devices fabricated in this study showed reliable electrical characteristics in the flat, bending (radius of 5 mm), and twist configurations (angle of up to $\sim 50^\circ$). Furthermore, the 3 μm -channel complementary inverters had reliable voltage transfer logic inverter operations in both the flat and twist configurations.

2. Experimental section

Fig. 1a shows the fabrication process of our micro-scale OFET devices using orthogonal photolithography. To fabricate the OFET devices, first, the PI substrate was cleaned using a standard solvent cleaning process using de-ionized

(DI) water and 2-propyl-alcohol (IPA) in an ultrasonic bath for 10 min at each cleaning. Next, the substrate was dried in a vacuum oven at 100 $^\circ\text{C}$ for 1 h to evaporate the residual solvent and moisture on the PI substrate. The bottom Al gate electrodes (30 nm thickness) were deposited by a thermal evaporator using a shadow mask with a deposition rate of 0.5 $\text{\AA}/\text{s}$ at a pressure of $\sim 10^{-6}$ torr. To prepare the polymeric dielectric layer, 15 wt% of poly (4-vinylphenol) (PVP) and 3 wt% of poly (melamine-co-formaldehyde) as a cross-linking agent were dissolved in a solvent of propylene glycol methyl ether acetate (PGMEA). After the UV-ozone treatment of the Al gate electrode/PI substrate for 10 min to improve the film uniformity and device reliability, the prepared PVP solution was spin-coated onto the Al gate electrode/PI substrate at 3000 rpm for 30 s, followed by soft-baking on a hot plate at 100 $^\circ\text{C}$ for 10 min in a N_2 -filled glove box. To enable the OFET devices to be electrically measured by probe tips, the portion of the PVP film on the pads of the Al gate electrode was removed with a methanol-soaked swab, followed by hard-baking on the hot plate at 200 $^\circ\text{C}$ for 40 min in a N_2 -filled glove box [27,28]. The thickness of the spin-coated PVP film was measured at ~ 1 μm using an Alpha-step profiler. To prepare the fluorinated photoresist solution, 10 wt% of the previously reported semi-perfluoroalkyl resorcinarene (denoted as R_F -Calix-tBoc, shown in Scheme 1a) and 0.5 wt% of an N-nonafluorobutanesulfonyloxy-1,8-naphthalimide photoacid generator (Scheme 1b) were dissolved in a mixed solvent (3-ethoxy-1,1,1,2,3,4,4,5,5,6,6,6-dodecafluoro-2-trifluoromethylhexane ((denoted as HFE 7500, shown in Scheme 1c); PGMEA = 4: 1 weight ratio), and then the mixed solution was filtered through a 0.20 μm -sized nylon syringe filter [19]. Afterwards, the fluorinated photoresist solution was spin-coated at 1500 rpm for 60 s onto the

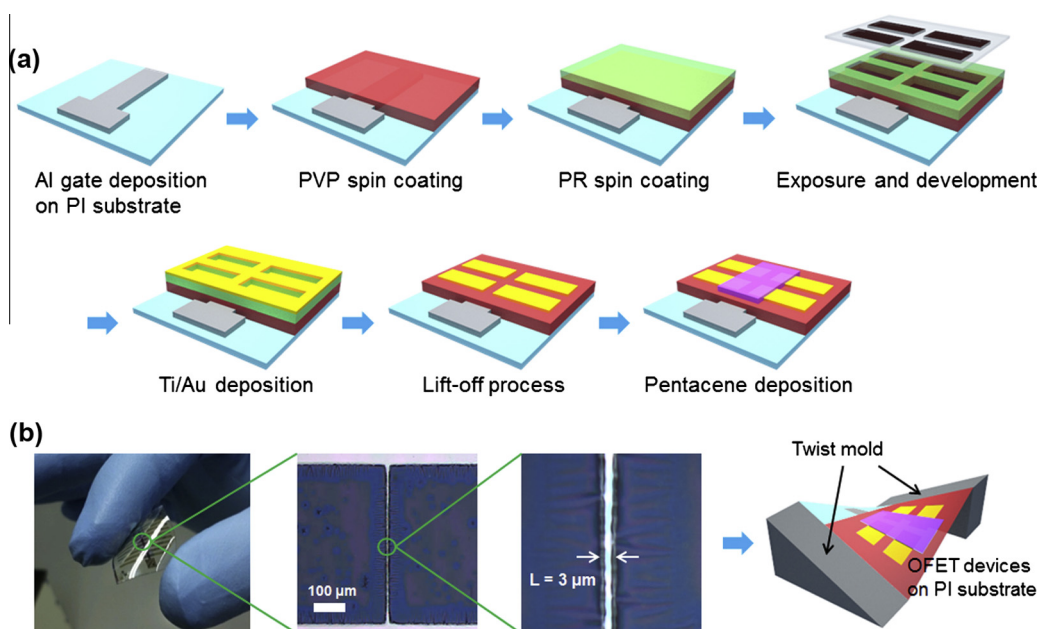
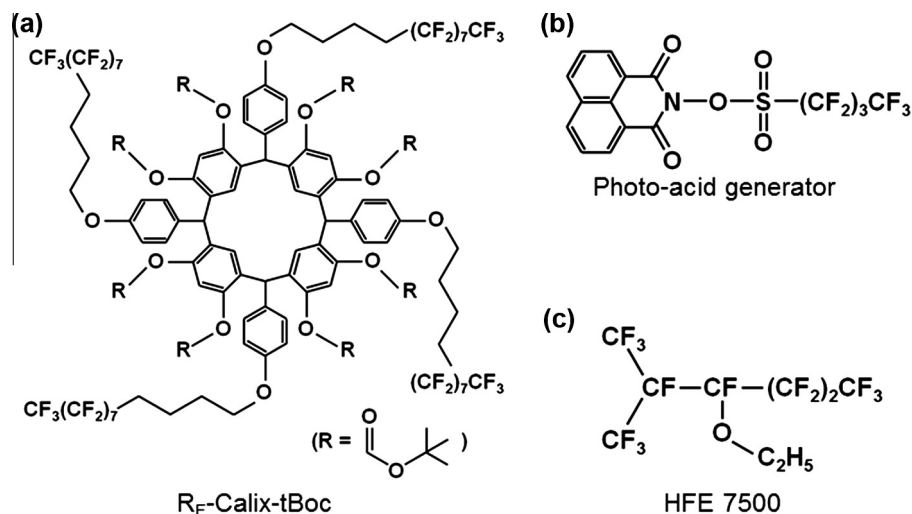


Fig. 1. (a) The fabrication process of our micro-scale twistable OFET devices on a flexible PI substrate by orthogonal photolithography. (b) Photographic and optical microscopic images of the OFET devices with a schematic illustration of the twisted OFET devices.



Scheme 1. The molecular structure of (a) semi-perfluoroalkyl resorcinarene of R_F -Calix-tBoc, (b) N-nonafluorobutanesulfonyloxy-1,8-naphthalimide photo-acid generator, and (c) fluorous solvent of HFE 7500 used in our highly fluorinated photoresist solution.

formed PVP film and baked on a hot plate at 75 °C for 3 min in a clean room under yellow light. Subsequently, the coated photoresist film was exposed to UV light (wavelength of 416 nm and intensity of $\sim 10 \text{ mW/cm}^2$) using a mask aligner with a chromium-patterned photo-mask, followed by an additional baking process at 75 °C for 3 min on the hot plate. In the development process, the unexposed region of the photoresist film below the chromium-drawn portion of the photo-mask was washed away by a development solvent of ethoxy-nonafluorobutane ($\text{C}_4\text{F}_9\text{OC}_2\text{H}_5$, denoted as HFE 7200), and the sample was dried with N_2 gas. Because our fluorinated photoresist has negative-tone photolithographic properties, the UV-exposed region of the photoresist film loses its solubility in the fluorous development solvent, whereas the unexposed portion can be removed by the development solvent, resulting in the formation of micro-scale development patterns without damaging the underlying PVP dielectric layer. To fabricate the source/drain electrodes, a Ti (5 nm thickness) adhesion layer and Au (30 nm thickness) electrodes were deposited on the developed samples using an electron beam evaporator with a deposition rate of 0.5 \AA/s at a pressure of $\sim 10^{-7}$ torr. Then, the unnecessary portion of the Ti/Au metal on the remaining photoresist film was washed away by using a lift-off solvent (HFE 7200: EtOH = 20: 1 weight ratio). During the lift-off process, only the Ti/Au layer directly deposited on the PVP film can remain, which plays a role as the source/drain electrodes, and the 3 μm -channel gap between the source/drain electrodes defines the channel length of our OFET devices. Finally, the pentacene (60 nm thickness) active layer was deposited using a thermal evaporator with a deposition rate of 0.5 \AA/s at a pressure of $\sim 10^{-6}$ torr. Fig. 1b shows the photographic and optical microscopic images of the 3 μm -channel OFET devices. In the case of the complementary inverters, an additional thermal evaporation process of an n-type F_{16} -CuPc layer was performed on the opposite region of the pentacene film, sharing the output voltage line by using a

shadow mask at the same deposition conditions as that of the p-type pentacene deposition. The electrical measurement of the OFET devices and complementary inverters was performed using a semiconductor analyzer system (Model 4200-SCS, Keithley, Inc.).

3. Results and discussion

Fig. 2 shows the electrical characteristics of our micro-scale pentacene OFET devices on the PI substrate under a flat condition. Fig. 2a displays the transfer curves (drain current versus gate voltage) of the 3 μm -channel pentacene OFET devices at a drain-source voltage of -40 V . The left axis (black curve) and right axis (blue curve) show the transfer curve as linear and log scale, respectively. The inset scheme in Fig. 2a shows the molecular structure of the pentacene material. Fig. 2b shows the output curves (drain current versus drain voltage) of the 3 μm -channel pentacene OFET devices for gate voltages from 20 to -40 V . Note that our devices showed somewhat low ON/OFF current ratio with high OFF current, which can be explained by the short channel geometry and relatively high contact resistance of the devices. Using orthogonal photolithography technique, we fabricated micro-scale short channel devices (channel length L of 3 μm) while maintaining the scale of channel width W (500 μm) to avoid the edge source contact and spreading current effect in the narrow channel transistors [29–31]. Therefore, the L/W ratio of the devices was very low, which resulted in short channel geometry. Because the pentacene bulk resistance is proportional to L/W ratio, the bulk resistance was also low, that is, the OFF current was somewhat high [32,33]. Nevertheless, the devices showed the stable electrical transfer properties and the obtained electrical properties were sufficient to operate the pentacene OFET devices. Because we fabricated the OFET devices by applying orthogonal photolithography on a polymer dielectric PVP film, it is important to check the quality of the PVP film

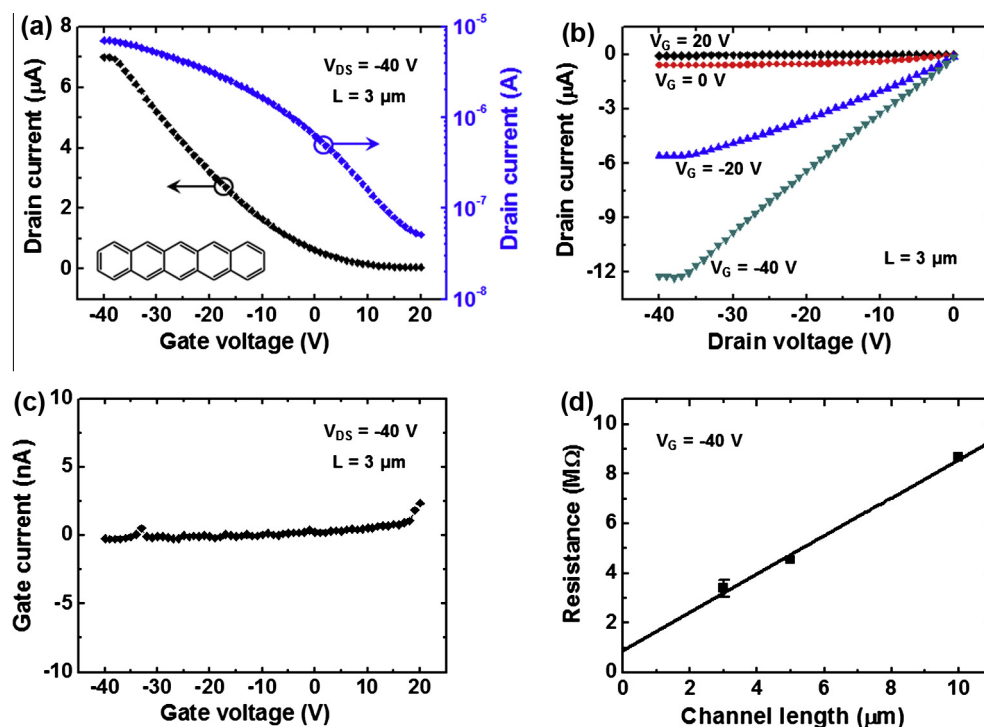


Fig. 2. (a) The transfer curves and (b) output curves of the 3 μm -channel OFET devices. (c) The gate leakage current in the transfer curve. (d) The series resistance versus various channel lengths of the OFET devices.

by examining the gate leakage current through the PVP film for the completely fabricated OFET devices. Fig. 2c shows that the gate leakage current in the gate voltage sweep was much lower than ~ 1 nA in most operating voltage ranges, which is a significantly lower value than the drain current level in Fig. 2a, indicating that the PVP film exhibited stable dielectric properties in our OFET devices. We also measured the electrical characteristics of the OFET devices that were fabricated with different channel lengths. Fig. 2d shows the linear dependence of the series resistance as a function of the channel length. Here, the series resistance values were obtained from the slope of the linear segments in the low drain voltage region (from 0 to -1 V) of the output curves. The contact resistance can be obtained as the y-intercept of the extrapolation fit of the series resistance versus the channel length data [34–36]. The obtained contact resistance was found to be ~ 1 M Ω , which is not much smaller than the series resistance of ~ 3.5 M Ω for the 3 μm -channel OFET devices due to the aforementioned short channel geometry [37]. Also, this may cause reduction of the field effect mobility of the devices, but the field effect mobility of our pentacene OFET devices exhibited a typical value (~ 0.1 cm 2 /V s) by considering other pentacene OFET devices of various device structures and fabrication conditions have showed mobility values in a range from 0.01 to 1 cm 2 /V s [38–40].

We also measured the electrical characteristics of the 3 μm -channel pentacene OFET devices in a bending configuration (radius of 5 mm) and after the bending 100 cycles, and the results are shown as the output curves in Fig. 3a

and b, respectively. The inset photographic image of Fig. 3a shows the OFET devices attached to a bending mold (radius of 5 mm) using a kapton tape. The inset of Fig. 3b shows the OFET devices in an automatic bending machine that counts the bending cycle numbers. Here, one bending number denotes one cycle from flat to bending and back to the flat configuration. Fig. 3c and d show the field effect mobility and threshold voltage (V_{TH}) values of the OFET devices, respectively, in the flat and bending conditions. These results indicate that the device performances (mobility of ~ 0.1 cm 2 /V s) were reliably maintained without serious degradation under the bending conditions. The error bars in all these plots were obtained by measuring the standard deviation of about 5 devices for each data point.

To ensure the practical flexibility of our OFET devices on a PI substrate, we measured the electrical characteristics of the OFET devices in twist configurations for various twist angles. For measuring the OFET devices in twist conditions, we placed two identical twist molds in the opposite direction of the inclined plane at a slightly smaller distance than the size of the PI substrate and attached the edge of the PI substrate to the edge of the inclined plane of each twist mold using the kapton tape (see Fig. 1b). Here, the twist angle is defined as angle between two oppositely directed inclined planes of twist molds. For instance, when we used two identical twist molds with inclined angle of 5° , the twist angle was determined as 10° in this twist configuration, and so did other twist angles. Thus, we twisted our OFET devices from a flat orientation to a twist angle of

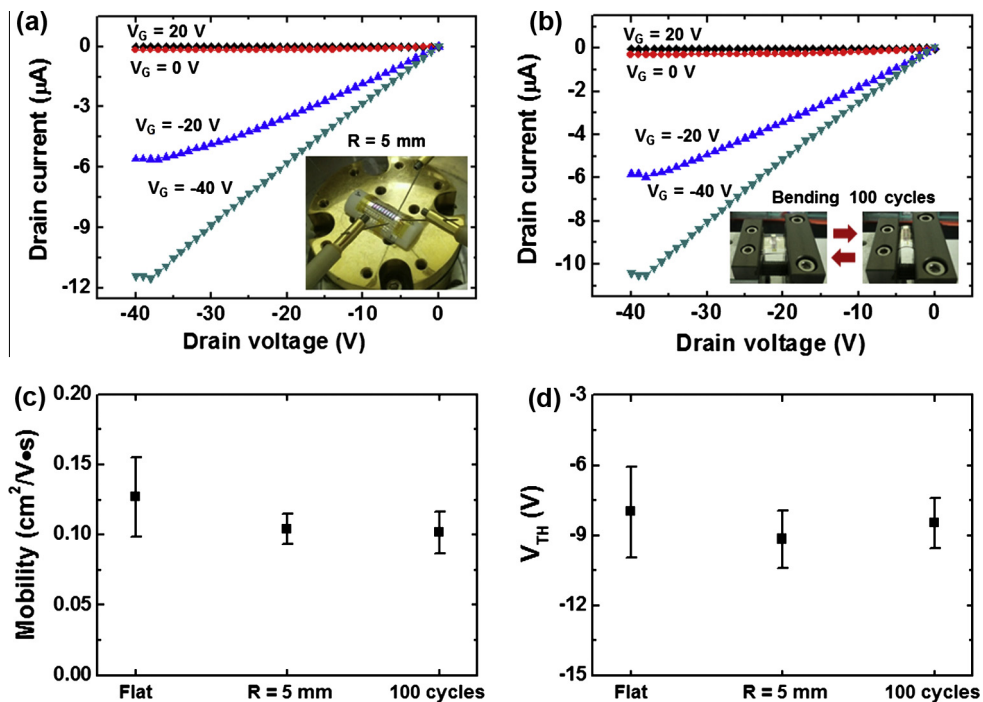


Fig. 3. The output curves of the 3 μm -channel OFET devices (a) in the bending configuration and (b) after the bending cycles. The inset photographic images show the OFET devices in each bending condition. (c) The field effect mobility and (d) threshold voltage (V_{TH}) values of the OFET devices are summarized for the flat and bending configurations and after the bending cycles.

50° with an increment angle of 10° . However, when the angle of twist reached 60° , the PI substrate was irreversibly folded, and no electrical characteristics were observed. Therefore, we assumed that 50° was the maximum twist angle of our OFET devices. Fig. 4a shows the output curves of the 3 μm -channel OFET devices in the twist configurations with angles from 10° to 50° . In this figure, the curves for each different twist angle are shown in different colors,

and the data for various gate voltages are represented by different symbol shapes. Because the threshold voltage of the OFET devices gradually decreased towards a more negative number due to the electrical degradation as the twist angles increased, the curves for $V_G = 20$ and 0 V appear particularly overlapped. Fig. 4b summarizes the field effect mobility and threshold voltage values of the OFET devices in the twist configurations. Although the device

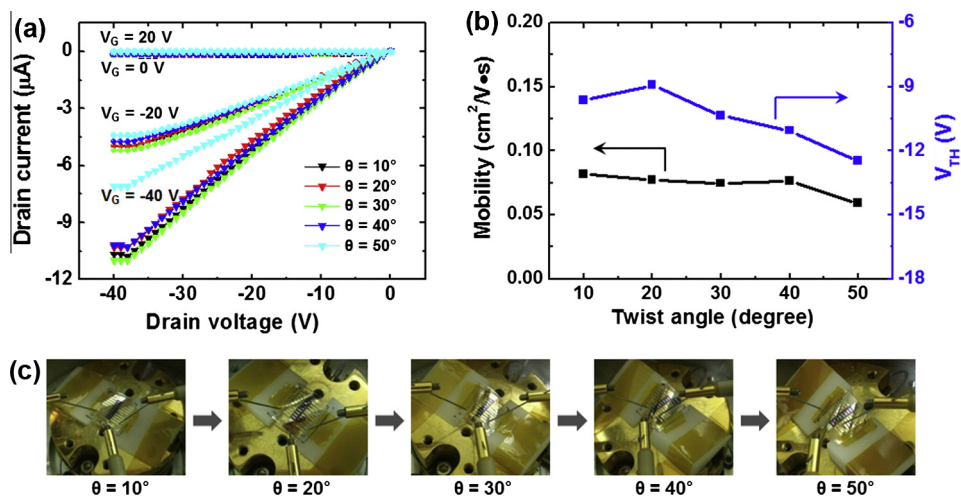


Fig. 4. (a) The output curves of the 3 μm -channel OFET devices in the twist configurations with a twist angle from 10° to 50° . (b) The field effect mobility and threshold voltage (V_{TH}) values of the OFET devices in the twist configurations with angles from 10° to 50° . (c) The photographic images of the OFET devices in each twist configuration.

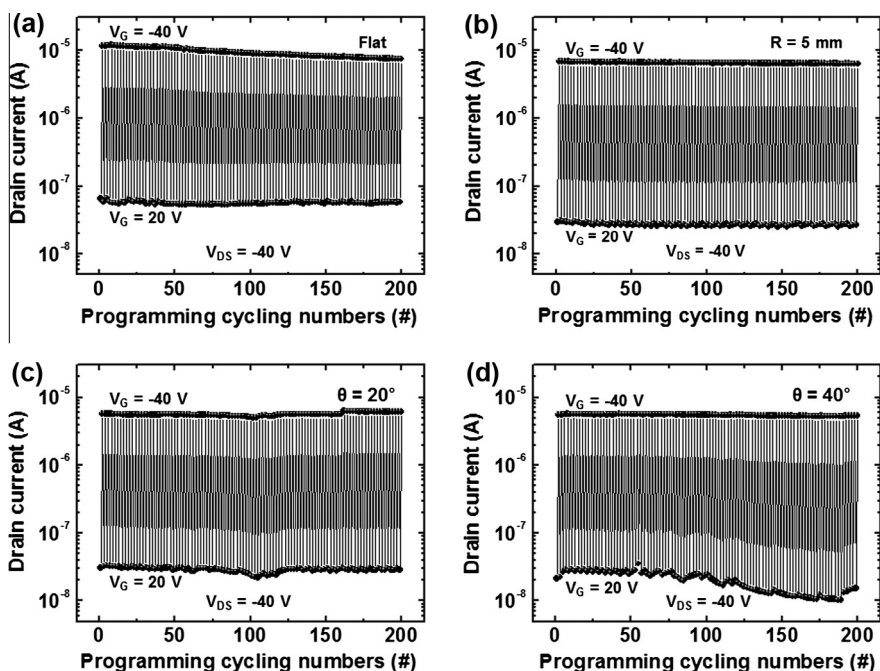


Fig. 5. DC sweep cycling endurance of the 3 μm -channel OFET devices from the repetitive gate voltage turning ON and OFF for the (a) flat, (b) bending (c) twisted by 20°, and (d) twisted by 40° configurations.

performances were slightly reduced as the twist angle increased to $\sim 50^\circ$ compared with the flat and bending conditions, the performance is sufficiently good to indicate that the overall characteristics were well maintained in the twist configurations. Fig. 4c shows the optical images of the OFET devices attached to the twist molds with the intended twist angles using kapton tape.

Fig. 5 shows the DC sweep cycling endurance of the 3 μm -channel OFET devices from the repetitive gate

voltage turning ON (-40 V) and OFF (20 V) at a drain-source voltage of -40 V under ambient conditions. During an endurance test of 200 cycles, the ON and OFF drain currents of the OFET devices were obtained in the flat (Fig. 5a), bending configuration of 5 mm (Fig. 5b), selected twist angle of 20° (Fig. 5c), and 40° (Fig. 5d). Although a slight fluctuation in the drain current was observed at the relatively high twist angle of 40°, the overall endurance characteristics of the ON/OFF ratio were well maintained in

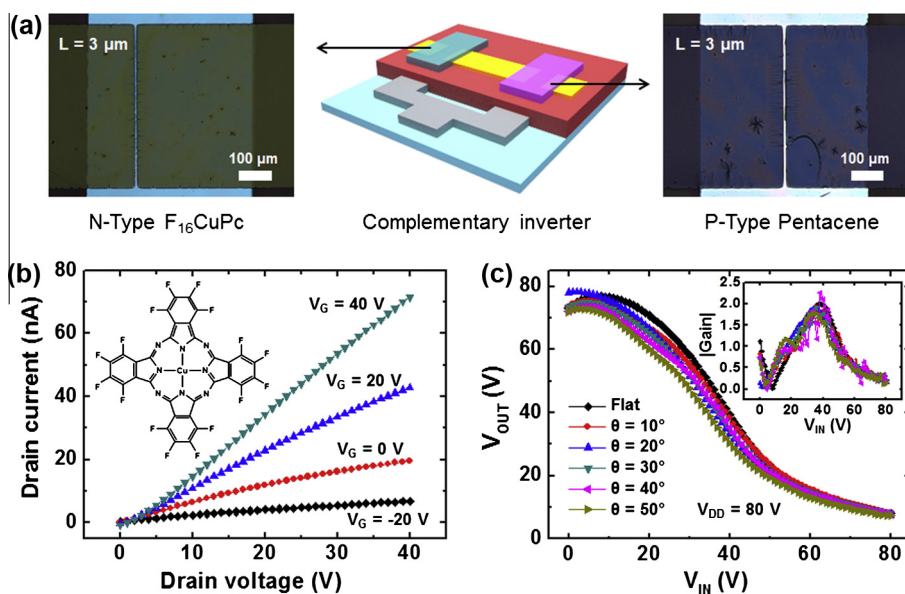


Fig. 6. (a) The schematic illustration and optical microscopic images of the 3 μm -channel complementary inverters. (b) The output curves of the n-type F_{16}CuPc OFET devices. (c) The voltage transfer curves of the complementary inverters in the flat and twist configurations with twist angles from 10° to 50° . The inset shows the voltage gain of the complementary inverters.

each flexible configuration. These results indicate that our micro-scale OFET devices have electrical and mechanical stability in various flexible configurations under bias stress in ambient conditions.

We also fabricated micro-scale twistable complementary inverters consisting of p-type pentacene and n-type $F_{16}CuPc$ materials (molecular structure is shown in Fig. 6b inset) on a flexible PI substrate by applying orthogonal photolithography as shown in the schematic and optical microscopic images of Fig. 6a. Because the $F_{16}CuPc$ material has excellent electrical and mechanical properties as an n-type semiconductor active layer, we used it here as an n-type active material for the complementary inverters, and the electrical characteristics as output curve are displayed in Fig. 6b [41,42]. Fig. 6c shows the voltage transfer curves for the logic inverter operations of our 3 μm -channel complementary inverters from flat to twist configurations with a twist angle of up to $\sim 50^\circ$ with the voltage gain of the complementary inverters (inset of Fig. 6c). The voltage gain of inverter is commonly defined as $|dV_{OUT}/dV_{IN}|$, which means this parameter is decided by abruptness of transition region in voltage transfer curves. Because the transfer curves of our pentacene OFET devices showed a little bit smooth property in the positive gate voltage region with negative threshold voltage, the voltage transfer curves also did. As a result, the maximum gain was not very large, but the peak points were well maintained at ~ 40 V in the voltage transfer characteristics under the twist configurations. Consequently, because of the compatibility between the pentacene and $F_{16}CuPc$ OFET devices for the electrical and mechanical properties, our micro-scale complementary inverters exhibited reliable logic inverter operations not only in flat configurations but also in complex flexible twist configurations.

4. Conclusions

In summary, we fabricated micro-scale twistable OFET devices and complementary inverters consisting of pentacene and $F_{16}CuPc$ on a flexible PI substrate by applying orthogonal photolithography using HFE development solvents and a compatible highly fluorinated photoresist solution containing a semi-perfluoroalkyl resorcinarene and photo-acid generator. The orthogonal photolithographic technology made it possible to fabricate the micro-scale organic devices on a flexible PI substrate without damaging the underlying polymer films. The fabricated 3 μm -channel pentacene OFET devices exhibited stable electrical characteristics in the flat condition, bending conditions (radius of 5 mm) and twist configurations (angle of up to $\sim 50^\circ$). Moreover, the 3 μm -channel complementary inverters were fabricated with p-type pentacene and n-type $F_{16}CuPc$ materials, and they exhibited reliable voltage transfer curves for the logic inverter operations in both flat and twist configurations.

Acknowledgements

The authors acknowledge the financial support from the National Creative Research Laboratory Program (Grant No.

2012026372) and the National Core Research Center (Grant No. 2008-0062606) through the National Research Foundation of Korea (NRF), which is funded by the Korean Ministry of Science, ICT & Future Planning. S.H. acknowledges the support from NRF Grant No. 2013M3C8A3078813, and J.-K.L. acknowledges the financial support from the Fundamental R&D Program for Core Technology of Materials (Grant # 10041220), which is funded by the Korean Ministry of Trade, Industry & Energy.

References

- [1] H. Klauk, *Organic Electronics 2: More Materials and Applications*, Wiley-VCH Verlag & Co. KGaA, Weinheim, 2012.
- [2] P. Peumans, S. Uchida, S.R. Forrest, *Nature* 425 (2003) 158.
- [3] J.C. Scott, L.D. Bozano, *Adv. Mater.* 19 (2007) 1452.
- [4] R.J. Tseng, J. Huang, J. Ouyang, R.B. Kaner, Y. Yang, *Nano Lett.* 5 (2005) 1077.
- [5] W. Cheng, Z. Wu, S. Wen, B. Xu, H. Li, F. Zhu, W. Tian, *Org. Electron.* 14 (2013) 2124.
- [6] G. Li, R. Zhu, Y. Yang, *Nat. Photonics* 6 (2012) 153.
- [7] H. Yan, Z. Chen, Y. Zheng, C. Newman, J.R. Quinn, F. Döt, M. Kastler, A. Facchetti, *Nature* 457 (2009) 679.
- [8] J.Y. Kim, K. Lee, N.E. Coates, D. Moses, T.-Q. Nguyen, M. Dante, A.J. Heeger, *Science* 317 (2007) 222.
- [9] Y.-Y. Noh, N. Zhao, M. Caironi, H. Sirringhaus, *Nat. Nanotechnol.* 2 (2007) 784.
- [10] Q.-D. Ling, D.-J. Liaw, C. Zhu, D.S.-H. Chan, E.-T. Kang, K.-G. Neoh, *Prog. Polym. Sci.* 33 (2008) 917.
- [11] S. Lee, M. Choi, S. Han, D. Choo, J. Jang, S. Kwon, *Org. Electron.* 9 (2008) 721.
- [12] D. Khim, K. Baeg, B. Yu, S. Kang, M. Kang, Z. Chen, A. Facchetti, D. Kim, Y.-Y. Noh, *J. Mater. Chem. C* 1 (2013) 1500.
- [13] T. Sekitani, K. Zaitsumi, Y. Noguchi, K. Ishibe, M. Takamiya, T. Sakurai, T. Someya, *IEEE Trans. Electron Dev.* 56 (2009) 1027.
- [14] H. Klauk, U. Zschieschang, J. Pflaum, M. Halik, *Nature* 445 (2007) 745.
- [15] W. Tang, L. Feng, J. Zhao, Q. Cui, S. Chen, X. Guo, *J. Mater. Chem. C* 2 (2014) 1995.
- [16] F. Li, A. Nathan, Y. Wu, B.S. Ong, *Organic Thin Film Transistor Integration: A Hybrid Approach*, Wiley-VCH Verlag & Co. KGaA, Weinheim, 2011.
- [17] A.A. Zakhidov, H. Fong, J.A. DeFranco, J.-K. Lee, P.G. Taylor, C.K. Ober, G.G. Malliaras, M. He, M.G. Kane, *Appl. Phys. Lett.* 99 (2011) 183308.
- [18] J.-K. Lee, M. Chatzichristidi, A.A. Zakhidov, P.G. Taylor, J.A. DeFranco, H.S. Hwang, H.H. Fong, A.B. Holmes, G.G. Malliaras, C.K. Ober, *J. Am. Chem. Soc.* 130 (2008) 11564.
- [19] A.A. Zakhidov, J.-K. Lee, J.A. DeFranco, H.H. Fong, P.G. Taylor, M. Chatzichristidi, C.K. Ober, G.G. Malliaras, *Chem. Sci.* 2 (2011) 1178.
- [20] J. Jang, Y. Song, H. Oh, D. Yoo, D. Kim, H. Lee, S. Hong, J.-K. Lee, T. Lee, *Appl. Phys. Lett.* 104 (2014) 053301.
- [21] W.-T. Tsai, *J. Hazard. Mater.* 119 (2005) 69.
- [22] A. Sekiya, S. Misaki, *J. Fluorine Chem.* 101 (2000) 215.
- [23] D.-H. Kim, J.-H. Ahn, W.M. Choi, H.-S. Kim, T.-H. Kim, J. Song, Y.Y. Huang, Z. Liu, C. Lu, J.A. Rogers, *Science* 320 (2008) 507.
- [24] W. Hyun, O. Park, B. Chin, *Adv. Mater.* 25 (2013) 4729.
- [25] K. Song, J. Noh, T. Jun, Y. Jung, H.-Y. Kang, J. Moon, *Adv. Mater.* 22 (2010) 4308.
- [26] S. Song, J. Jang, Y. Ji, S. Park, T.-W. Kim, Y. Song, M.-H. Yoon, H.C. Ko, G.-Y. Jung, T. Lee, *Org. Electron.* 14 (2013) 2087.
- [27] Y. Ji, M. Choe, B. Cho, S. Song, J. Yoon, H. Ko, T. Lee, *Nanotechnology* 23 (2012) 105202.
- [28] S. Chung, J. Jeong, D. Kim, Y. Park, C. Lee, Y. Hong, *J. Display Technol.* 8 (2012) 48.
- [29] L. Mariucci, M. Rapisarda, A. Valletta, S. Jacob, M. Benwadih, G. Fortunato, *Org. Electron.* 14 (2013) 86.
- [30] F. Faccio, G. Cervelli, *IEEE Trans. Nucl. Sci.* 52 (2005) 2413.
- [31] L. Wang, D. Fine, T. Jung, D. Basu, H. Seggern, A. Dodabalapur, *Appl. Phys. Lett.* 85 (2004) 1772.
- [32] J.N. Haddock, X. Zhang, S. Zheng, Q. Zhang, S.R. Marder, B. Kippelen, *Org. Electron.* 7 (2006) 45.
- [33] K. Tsukagoshi, F. Fujimori, T. Minari, T. Miyadera, T. Hamano, Y. Aoyagi, *Appl. Phys. Lett.* 91 (2007) 113508.
- [34] C. Kim, Y. Bonnassieux, G. Horowitz, *IEEE Trans. Electron Dev.* 60 (2013) 280.

- [35] K. Fukuda, Y. Takeda, M. Mizukami, D. Kumaki, S. Tokito, *Sci. Rep.* 4 (2014) 3947.
- [36] S. Lee, G. Jo, S.-J. Kang, G. Wang, M. Choe, W. Park, D.-Y. Kim, Y.H. Kahng, T. Lee, *Adv. Mater.* 23 (2011) 100.
- [37] J. Zaumseil, K.W. Baldwin, J.A. Rogers, *J. Appl. Phys.* 93 (2003) 6117.
- [38] P.V. Pesavento, K.P. Puntambekar, C.D. Frisbie, J.C. McKeen, P.P. Ruden, *J. Appl. Phys.* 99 (2006) 094504.
- [39] Y. Kato, S. Iba, R. Teramoto, T. Sekitani, T. Someya, H. Kawaguchi, T. Sakurai, *Appl. Phys. Lett.* 84 (2004) 3789.
- [40] G. Horowitz, *Adv. Mater.* 10 (1998) 365.
- [41] S.D. Vusser, S. Steudel, K. Myny, J. Genoe, P. Heremans, *Appl. Phys. Lett.* 88 (2006) 162116.
- [42] Z. Bao, *Adv. Mater.* 12 (2000) 227.